Nuclear Science and Techniques (2025) 36:61
https://doi.org/10.1007/s41365-025-01646-y

Modified logistic nanodosimetry model for calculating relative biological effectiveness

Jing-Fen Yang[1,2,3,4] · Xin-Guo Liu[1,2,3,4] · Hui Zhang[1,2,3,4] · Peng-Bo He[1,2,3,4] · Yuan-Yuan Ma[1,2,3,4] · Guo-Sheng Shen[1,2,3,4] · Wei-Qiang Chen[1,2,3,4] · Qiang Li[1,2,3,4]

Received: 2 February 2024 / Revised: 28 April 2024 / Accepted: 13 May 2024 / Published online: 23 February 2025

Abstract

DNA double-strand breaks (DSBs) may result in cellular mutations, apoptosis, and cell death, making them critical determinants of cellular survival and functionality, as well as major mechanisms underlying cell death. The success of nanodosimetry lies in the reduction in the number of modeling parameters to be adjusted for the model to predict experimental data on radiation biology. Based on this background, this study modified and simplified the logistic nanodosimetry model (LNDM) based on radiation-induced DSB probability. The probability distribution of ionization cluster size $P(\nu|Q)$ under irradiation with carbon-ion beams was obtained through a track-structure Monte Carlo (MC) simulation, and then, the nanodosimetric quantities and DSB probability were calculated. Combining the assumptions of the linear quadratic (LQ) model and LNDM, DSB probability-based modification and simplification of the LNDM were conducted. Additionally, based on the radiobiological experimental data of human salivary gland (HSG), Chinese hamster lung (V79), and Chinese hamster ovary (CHO-K1) cells, the least-squares method was used to optimize the parameters of the modified LNDM (mLNDM). The mLNDM accurately reproduced the experimental data of HSG, V79, and CHO-K1 cells, and the results showed that the model parameters r and m_0 were independent of the cell type, that is, the biological effects of cells with different radiosensitivities can be characterized by adjusting only the model parameters k and $P_{s\to l}$. Compared with HSG and CHO-K1 cells, V79 cells had smaller k and $P_{s\to l}$ values, indicating that that DSBs have a lower probability of eventually causing lethal damage, and sublethal events are less likely to interact to form lethal events, thereby having radioresistant characteristics. Compared with the LNDM, the mLNDM eliminates the tedious derivation process and connects the quantities characterizing radiation quality at the nanoscale level using radiation biological effects in a more direct and easy-to-understand manner, thus providing a simpler and more accurate method for calculating relative biological effectiveness for ion-beam treatment planning.

Keywords Nanodosimetry · DNA double-strand break probability · Biophysical model · Carbon-ion radiotherapy

1 Introduction

Ion beams are considered to be the most promising radiation type for radiotherapy owing to their inverted depth-dose distribution and high relative biological effectiveness (RBE) near the Bragg peak. The Institute of Modern Physics (IMP),

This work was supported by the National Key Research and Development Program of China (No. 2022YFC2401503), Key Research and Development Program of Gansu Province (No. 23YFFA0010), Natural Science Foundation of Gansu Province (No. 23JRRA625), and Special Project of Science and Technology Cooperation between Hubei Province and Chinese Academy of Sciences (No. 420000021817T300000050).

✉ Qiang Li
liqiang@impcas.ac.cn

[1] Institute of Modern Physics, Chinese Academy of Sciences, Lanzhou 730000, China

[2] Key Laboratory of Heavy Ion Radiation Biology and Medicine of Chinese Academy of Science, Lanzhou 730000, China

[3] Key Laboratory of Basic Research on Heavy Ion Radiation Application in Medicine, Lanzhou 730000, China

[4] University of Chinese Academy of Sciences, Beijing 100049, China

Chinese Academy of Sciences, has been conducting basic research on heavy-ion cancer therapy since 1995 [1]. In terms of the biological effects and mechanisms of heavy-ion radiation, IMP researchers have conducted experiments at various levels, including molecule, *in vitro* cell culture, and animal studies [2]. For the techniques of heavy-ion therapy, two-dimensional (2D), two-dimensional plus layer-stacking (2D-LS), and three-dimensional (3D) conformal irradiation methods, treatment planning systems, and spot-scanning beam delivery have been developed [3–5]. Regarding the early clinical trial research on heavy-ion therapy, IMP has used carbon-ion beams provided by the Heavy Ion Research Facility in Lanzhou (HIRFL) to conduct preliminary clinical trials of heavy-ion therapy for 103 shallow- and 110 deep-seated tumor patients between 2006 and 2013 [6]. Since then, China has become the fourth largest country in the world, after the USA, Japan, and Germany, with the ability to implement heavy-ion cancer therapy [7, 8].

Unlike the use of physical absorbed doses for treatment planning and plan evaluation in photon radiotherapy, ion-beam therapy often employs the RBE-weighted dose (RWD), the product of the RBE value and physical absorbed dose [9]. The RBE value is significantly influenced by many physical and biological factors, such as ion type, energy, physical absorbed dose, linear energy transfer (LET), cell type, and biological endpoint [10, 11]. Obtaining RBE values for all clinical conditions in radiobiological experiments is difficult or impossible. Therefore, establishing an accurate biophysical model to predict the RBE value is a prerequisite for treatment planning in ion-beam radiotherapy. Currently, the biophysical models used in different particle therapy centers include the mixed-beam model [12], microdosimetric kinetic model (MKM) [13], and local effect model (LEM) [14]. In addition, the logistic nanodosimetry model (LNDM) was established by Dai et al. [15] in 2020, which achieved a leap in ion-beam RBE calculation from the microscale to nanoscale and improved the accuracy and reliability of the ion-beam RBE model.

The LNDM is based on ionization cluster size distribution (ICSD), and it assumes that radiation-induced cell death can be divided into two types: Direct and indirect lethal events. When at least two ionizations exist within the nanoscale cell nucleus domain, it can be transformed into a direct lethal event. The combination of sublethal events can result in indirect lethal events. Based on these assumptions, a series of formulas was derived using the first moment of the conditional cluster size distribution with an ionization cluster size ICS ≥ 1 ($M_1^{C_1}$), the first moment of the conditional cluster size distribution with ICS ≥ 2 ($M_1^{C_2}$), and the cumulative probabilities with ICS ≥ 2 ($F_2^{C_1}$). Subsequently, the nanodosimetric RBE calculation model was constructed. In the LNDM, the mathematical formula for the natural logarithm of the cell survival fraction is given by the linear quadratic (LQ) model. The logistic function is introduced into the model to adequately describe the overkill effect in a high-LET region. A good agreement was observed between the RBE values calculated using the model and experimental data.

Regardless of the intermediate processes of radiobiological effects in the chemical and biochemical stages, a direct link exists between random ionization in the early stages and the measurable biological effects in the later stages [16–19]. Scientific skepticism and concerns exist regarding the assertion that interactions within individual nanovolume elements exclusively determine the fate of irradiated tissues or cells. Fortunately, several scholars have established models for predicting radiation-induced DNA damage by correlating nanodosimetry with DNA damage, indicating that the ICSD is the main basis for determining DNA strand breaks [20]. The results showed that the DNA damage yield can be predicted according to the ICSDs, and for protons with different energies, the model predictions were in good agreement with Monte Carlo (MC) simulation results. However, the prediction of biological endpoints was limited to initial DNA damage rather than more complex cellular endpoints to accommodate the limited available nanodosimetric quantities and radiobiological experimental data obtained under the same radiation conditions in the previous study.

In addition, while nanodosimetry has demonstrated some success in correlating physical quantities measured at the nanometer level using radiobiological outcomes [21], the same can be said for microdosimetry to a certain extent [22]. The actual success of nanodosimetry lies in its reduction of the number of modeling parameters that must be adjusted for the model to predict radiation biology data. However, the LNDM still requires the tuning of four parameters, similar to the MKM. Thus, the modeling parameters required to calculate RBE values should be reduced in a more direct manner.

In this study, the LNDM was modified. First, the size distribution of the DNA damage clusters was calculated according to the ICSD derived from track-structure MC simulations. Subsequently, considering the probability of DNA double-strand breaks (DSBs) and LNDM assumptions, a DNA damage probability-based modification for the LNDM was conducted to form a modified LNDM (mLNDM). Moreover, to reduce the number of model parameters, when optimizing the model parameters for different cell lines, we attempted to fix some model parameters to identify those that are not related to cellular radiosensitivity. In this study, we assessed cell death caused by radiation-induced DNA damage at the nanoscale, and number of parameters of the mLNDM was reduced, which is crucial for an easy understanding of the relationship between nanodosimetry and radiation biological effects.

2 Materials and methods

2.1 Calculation of DSB probability

The most sensitive target of radiation in tissues is the genetic material, DNA, and its damage can cause mutations and cell death. In particular, a DSB is the most basic and severe form of DNA damage, which can elicit the loss of DNA template function, and is the main cause of chromosomal aberrations and cell death. However, the LNDM, the ion-beam RBE model based on ICSD, explores only the relationship between nanodosimetric quantities and cell survival but does not include DNA damage. Previous studies have established models correlating ICSD with DNA damage yield and demonstrated that the model can well predict the DNA damage yield caused by ionizing radiation [20]. The following is a brief description of the model.

Assuming that ν is the number of radiation-induced ionizations within a nanoscopic sensitive volume and each ionization causes at most one strand break in DNA, the probability of ν ionizations creating n_{SB} strand breaks can be defined as follows:

$$P_{\mathrm{SB}}\left(n_{\mathrm{SB}}|\nu\right)=\binom{\nu}{n_{\mathrm{SB}}}p_{\mathrm{SB}}^{n_{\mathrm{SB}}}\left(1-p_{\mathrm{SB}}\right)^{\nu-n_{\mathrm{SB}}}, \tag{1}$$

where p_{SB} is the probability of converting each ionization into a strand break. Note that p_{SB} is essentially a radiochemical parameter. Its value depends on the chemical reaction kinetics of the initial water radiolysis products in a DNA-scavenging environment and is independent of the radiation field and cell type. The subsequent cascade of cellular signaling and repair responses may be responsible for the large variations in the intrinsic radiosensitivity. $p_{\mathrm{SB}}=0.15$ is used in this paper [23].

$P(\nu|Q)$ represents the probability of particles with radiation quality Q producing ν ionizations within the target volume at nanometer scale. Thus, the probability distribution of the ICSD resulting in n_{SB} strand breaks in the DNA segment is

$$f_{\mathrm{SB}}\left(n_{\mathrm{SB}}\right)=\sum_{\nu=1}^{\nu=10}P(\nu|Q)P_{\mathrm{SB}}\left(n_{\mathrm{SB}}|\nu\right). \tag{2}$$

Large ICSs not only occur with low probability, but also have a poor effect of complex damage owing to radiation-induced recombination of free radicals, which is not conducive to describing radiobiological effects [24]. Therefore, ICS >10 is ignored in the calculation process [25].

Further analysis shows that not all n_{SB} strand breaks occur on the same DNA strand. A probability $p_{\mathrm{DSB}}\left(n_{\mathrm{SB}}\right)=1-\left(\frac{1}{2}\right)^{n_{\mathrm{SB}}-1}$ exist that n_{SB} strands combine DSBs. Thus, the probability distribution of DSB caused by n_{SB} strand breaks is

$$f_{\mathrm{DSB}}\left(n_{\mathrm{SB}}\right)=\sum_{\nu=2}^{\nu=10}P(\nu|Q)P_{\mathrm{SB}}\left(n_{\mathrm{SB}}|\nu\right)p_{\mathrm{DSB}}\left(n_{\mathrm{SB}}\right). \tag{3}$$

The cumulative probability of the DSB can be calculated as

$$F_{\mathrm{DSB}}=\sum_{n_{\mathrm{SB}}=2}^{n_{\mathrm{SB}}=10}\sum_{\nu=n_{\mathrm{SB}}}^{\nu=10}P(\nu|Q)P_{\mathrm{SB}}\left(n_{\mathrm{SB}}|\nu\right)p_{\mathrm{DSB}}\left(n_{\mathrm{SB}}\right). \tag{4}$$

2.2 Modification of the LNDM

The relationship between the cell survival fraction and physical absorbed dose is expressed as a well-known LQ model [26, 27] as follows:

$$-\ln S=\alpha D+\beta D^2, \tag{5}$$

where α reflects the cell death generated by direct hitting; the number of cell deaths induced by this method is proportional to the physical absorbed dose. β describes cell death due to the accumulation of damages; the number of cell deaths caused in this manner is proportional to the square of the physical absorbed dose.

The LNDM considers two types of radiation-induced cell deaths: direct and indirect lethal events resulting from a combination of sublethal events. Note that direct and indirect lethal events in the LNDM are different from the concepts in the theory of dual-radiation action. A direct lethal event alone can result in cell death by introducing unrepairable lesions, whereas a single sublethal event cannot cause cell death on its own but must interact with another neighboring event to form an indirect lethal event. Corresponding to the LQ model, α and β have the same meaning in the modification of the LNDM, that is, direct and indirect lethal events, respectively.

In the mLNDM, a direct lethal event is possible only if at least one DNA DSB exists in the nanoscale target volume. For a cell nucleus containing N ionizations, the number of direct lethal events occurring within the cell is expressed as follows:

$$L_{\mathrm{D}}=\frac{N}{M_1^{C_1}}\cdot F_{\mathrm{DSB}}P\left(M_1^{C_1}\right), \tag{6}$$

where $P\left(M_1^{C_1}\right)$ is the probability of eventual transformation of the DSBs within a target volume of DNA into a lethal event and can be expressed as a logistic function. In contrast to the original LNDM, it is the function of $M_1^{C_1}$. With the increase in $M_1^{C_1}$, $P\left(M_1^{C_1}\right)$ increases until it reaches saturation. $P\left(M_1^{C_1}\right)$ is calculated as follows:

$$P\left(M_1^{C_1}\right) = \frac{k}{1+\exp\left[-r\left(M_1^{C_1}-m_0\right)\right]}, \tag{7}$$

$M_1^{C_2}$ in the original model is replaced with $M_1^{C_1}$ to reduce the number of nanodosimetric quantities associated with the biological effects of radiation in the model.

The first moments of the conditional ICS distributions with $\nu \geq 1$ and $\nu \geq 2$ are defined as follows.

$$M_1^{C_1}(Q) = \sum_{\nu=1}^{\infty} \nu \cdot \frac{P(\nu|Q)}{\sum_{\nu=1}^{\infty} P(\nu|Q)} \tag{8}$$

$$M_1^{C_2}(Q) = \sum_{\nu=2}^{\infty} \nu \cdot \frac{P(\nu|Q)}{\sum_{\nu=2}^{\infty} P(\nu|Q)} \tag{9}$$

The original LNDM involves nanodosimetric quantities such as $M_1^{C_1}$, $M_1^{C_2}$ and $F_2^{C_1}$, whereas the mLNDM incorporates nanodosimetric quantities, specifically $M_1^{C_1}$ and F_{DSB}. Therefore, one nanodosimetric quantity is reduced in the mLNDM. The use of a minimal number of nanodosimetric quantities to describe the biological effects of radiation facilitates the exploration of the optimal nanodosimetric quantity for characterizing the radiation quality of carbon-ion beams and enhances the understanding of the model.

The target volumes containing DSBs without eliciting lethal events and those containing multiple single strand breaks can result in sublethal events. The number of sublethal events is

$$L_{\mathrm{sub}} = \frac{N}{M_1^{C_1}} \cdot \left[1 - F_{\mathrm{DSB}} P\left(M_1^{C_1}\right)\right]. \tag{10}$$

Indirect lethal events are caused by the accumulation of sublethal events. Therefore, they are proportional to the square of the number of sublethal events:

$$L_{\mathrm{I}} = L_{\mathrm{sub}}^2 \cdot P_{s\to l}, \tag{11}$$

$$L_{\mathrm{I}} = \left(\frac{N}{M_1^{C_1}}\right)^2 \left[1 - F_{\mathrm{DSB}} P\left(M_1^{C_1}\right)\right]^2 \cdot P_{s\to l}, \tag{12}$$

where $P_{s\to l}$ is the probability of generating indirect lethal events owing to the accumulation of sublethal events.

The total number of ionization events N undergoes the following transformation relationship with the specific energy z:

$$N = z\rho V/\omega, \tag{13}$$

where ρ and V are the cell nucleus density and volume, respectively, and ω is the mean ionization energy.

The expected value of the specific energy z is the macroscopic physical absorbed dose; thus,

$$N = D\rho V/\omega. \tag{14}$$

Thus, the number of direct lethal events can be expressed as

$$L_{\mathrm{D}} = \frac{D\rho V}{\omega M_1^{C_1}} \cdot F_{\mathrm{DSB}} P\left(M_1^{C_1}\right). \tag{15}$$

Subsequently, the coefficient parameter α of the LQ model is

$$\alpha = \frac{\rho V}{\omega M_1^{C_1}} \cdot F_{\mathrm{DSB}} P\left(M_1^{C_1}\right). \tag{16}$$

The number of indirect lethal events is expressed as follows:

$$L_{\mathrm{I}} = \left(\frac{D\rho V}{\omega M_1^{C_1}}\right)^2 \left[1 - F_{\mathrm{DSB}} P\left(M_1^{C_1}\right)\right]^2 \cdot P_{s\to l}. \tag{17}$$

Subsequently, β is:

$$\beta = \left(\frac{\rho V}{\omega M_1^{C_1}}\right)^2 \left[1 - F_{\mathrm{DSB}} P\left(M_1^{C_1}\right)\right]^2 \cdot P_{s\to l}. \tag{18}$$

The RBE value is calculated as follows:

$$RBE = \frac{D_{\mathrm{X}}}{D_{\mathrm{Carbon}}} = \frac{2\beta D_{\mathrm{X}}}{\sqrt{\alpha^2 - 4\beta \ln S} - \alpha}. \tag{19}$$

2.3 Determination of modeling parameters

Before applying the model, the free parameters k, r, m_0 and $P_{s\to l}$ in the mLNDM must be determined, where k, r, and m_0 are parameters of the logistic function. k controls the scaling factor. r and m_0 modulate the growth rate and position on the horizontal axis, respectively. The optimization of the mLNDM parameters is primarily based on radiobiological experimental data reported by Furusawa et al. [28] and Weyrather et al. [29] using the least-squares method. To reduce the number of model parameters, we optimized the model parameters for different cell lines to fix some parameters to determine the most relevant ones to the cell lines. The other relevant data involved in the model, ρ, V, and ω, were 1 g/cm^3, 523.3 μm^3, and 33 eV, respectively.

Consistent with the experimental conditions reported by Furusawa et al. [28], a carbon-ion beam of 135 MeV/u was used in this study to calculate the ICSD. First, based on TOPAS [30], the phase space files were scored at the entrance of 1 mm-thick slices under the irradiation conditions of investigation (at different water-equivalent depths for different LET values) using the physics lists "g4em-standard_opt4", "g4decay", "g4ion-binarycascade",

"g4h-elastic_HP", "g4stopping", and "g4ion-QMD" [31]. The phase space scorers included the particle position, angle of incidence, energy, weight, and type. Second, based on TOPAS-nBio [32], the ICSDs were calculated using track-structure MC simulations. Among them, the simplified chromatin fiber model of DNA proposed by Bueno et al [33] was introduced. 1800 small cylinders with a diameter of 2.3 nm and height of 3.4 nm were uniformly, randomly, and non-overlappingly distributed in a large cylinder with a diameter of 30.4 nm and a height of 161 nm. The small cylinders were the volume elements at nanoscale level, corresponding to DNA segments of 10 base pairs, and a large cylinder corresponded to a chromatin filament. The introduction of the large cylinder ensured reasonable statistical accuracy within an acceptable computation time. The particles in the phase space were incident on the center of one of the end caps of the large cylinder, with the incident angle from the phase space data. In the macroscopic simulations, the lateral extent of the beam was fully contained in the phase-space files such that the coordinates of all particles in phase space collapsed at the same point on the track-structure simulations. The physics process applied was "g4em-dna." To ensure electron equilibrium, we placed the above-mentioned large cylinder containing 1800 nanometric volume elements in the center of a cubic box of 200 nm×200 nm×200 nm.

For the experimental conditions reported by Weyrather et al. [29], monoenergetic carbon-ion beams were applied. Carbon-ion beams with energies of 266.4, 190.7, 76.9, 18.0, 11.0, 5.4, 4.2, and 2.4 MeV/u were, respectively, incident on the chromatin filament. The computational simulations of subsequent ICSDs were consistent with the process as mentioned previously.

3 Results

3.1 Distributions of ICS and DNA damage cluster size

The ICSDs at different LETs located at different penetration depths of the carbon-ion radiation field are shown in Fig. 1. These data were acquired by irradiating a simplified chromatin fiber model of DNA with a 135 MeV/u carbon-ion beam, the same as that used to obtain the experimental data. The larger the LET, the larger the maximum ICS could be generated. The probability distributions of SB and DSB were obtained by substituting the ICSDs into Eqs. (2) and (3). Figure 2 shows the calculated probability distributions of SB and DSB for different LETs. Subsequently, the cumulative probability of DSB could be obtained using Eq. (4).

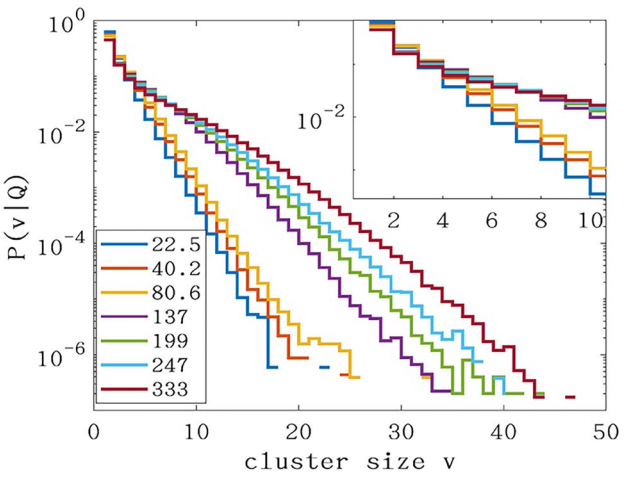

Fig. 1 (Color online) Probability distributions of ICS at the LET values of 22.5, 40.2, 80.6, 137, 199, 247, and 333 keV/μm for the radiation field of the 135 MeV/u carbon-ion beam

3.2 Model parameters

The mLNDM parameters for human salivary gland (HSG), Chinese hamster lung (V79), and Chinese hamster ovary (CHO-K1) cells are shown in Table 1. The free parameters r and m_0 were set to be independent of cell type; that is, they were independent of cell radiosensitivity. The parameter k could adequately describe the radiosensitivity of cells. Compared with HSG and CHO-K1 cells, V79 cells had a smaller k value, suggesting that the probability of lethal events caused by DNA DSBs was low for V79 cells. V79 cells probably had a stronger ability to repair DNA damages and thus had radioresistance. $P_{s\to l}$ was also a parameter reflecting the radiosensitivity of the cells. The $P_{s\to l}$ value of V79 cells was smaller than those of HSG and CHO-K1 cells, indicating that the sublethal events in V79 cells were less likely to induce lethal events, thereby exhibiting radioresistance.

The results demonstrated that the free parameters r and m_0 can be independent of the cell type and have fixed values in the mLNDM. The free parameters that truly characterize cell radiosensitivity in the mLNDM were k and $P_{s\to l}$, as only two free parameters must be adjusted when predicting the RBE values, which is useful for understanding the relationship between DNA damage at the nanoscale level and the biological effects of radiation.

3.3 Comparison of the mLNDM, LNDM, and experimental data

The coefficients α and β of the LQ model for HSG, V79, and CHO-K1 cells in different LET mixed radiation fields were predicted using the best fitting model parameters. The

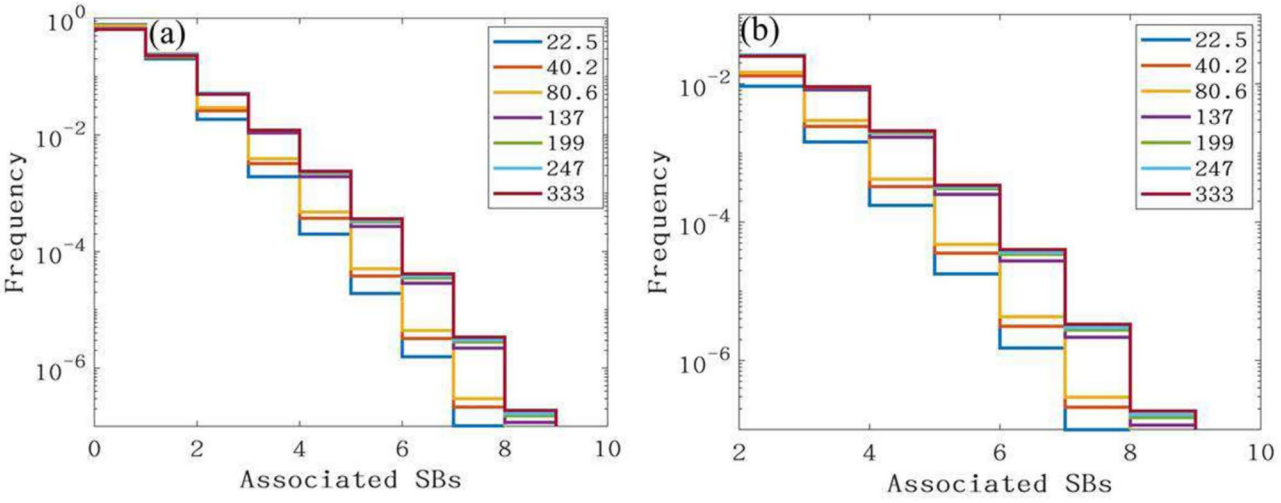

Fig. 2 (Color online) Probability distributions of SB (**a**) and DSB (**b**) at the LET values of 22.5, 40.2, 80.6, 137, 199, 247, and 333 keV/μm for the radiation field of the 135MeV/u carbon-ion beam

Table 1 mLNDM parameters for HSG, V79, and CHO-K1 cells

	r	m_0	k	$P_{s\to l}$
HSG	8.04	1.69	1.30×10^{-3}	2.23×10^{-11}
V79			9.59×10^{-4}	9.02×10^{-12}
CHO-K1			1.20×10^{-3}	1.62×10^{-11}

comparison between the predicted results for the mLNDM and LNDM and the experiment-derived data is shown in Fig. 3. The α coefficient of the LQ model increased with increasing LET values, and when the LET reached a certain value, it decreased as the LET value increased. The β coefficient of the LQ model decreased with the increase in the LET value. The agreement between the parameters of LQ model calculated using the mLNDM and the experimental data was good.

The dependences of RBE calculated by the mLNDM and LNDM on LET for HSG, V79, and CHO-K1 cells are shown in Fig. 4. Clearly, the trend of RBE with LET was well described by the mLNDM, particularly the overkill effect in high-LET mixed radiation fields. The determination coefficients R^2 of the experimentally derived data and calculated α, β and RBE values from mLNDM and LNDM are listed in Table 2.

4 Discussion

The original LNDM was proposed and preliminarily validated using cell experimental data from a study previously published by our team [15]. Compared with existing models, the LNDM for the first time used ICSD information to calculate the ion-beam RBE value and achieved a leap in ion-beam RBE calculation from the microscale to nanoscale. The LNDM provides a new method for calculating the RBE values of ion beams. The essence of the ion-beam RBE is associated with the microscopic track structure of charged particles because of the significant effect of cell death induced by ionizing radiation damages the cell nucleus, particularly the DNA molecules in the cell nucleus, indicating that the interaction between radiation and cells has been targeted at the nanoscale [34, 35]. Therefore, the development of nanoscale ion-beam RBE computational models may be a trend. The LNDM lays the foundation for the development of RBE calculation methods at the nanoscale. In this study, the LNDM was further optimized based on the distribution of DNA strand breaks, and we preliminarily proved that two of the four parameters in the mLNDM were independent of the cell type, indicating that the biological effects of different cell radiosensitivities can be characterized by adjusting only the two parameters, establishing an easy-to-understand RBE calculation method for carbon-ion beams.

As the carrier of genetic information, DNA is an important biological target molecule for radiation-induced cell death and mutations. Among all biological effects of radiation, nuclear DNA damage is the most significant. From a microscopic perspective, nuclear DNA is useful for understand the relationship between ionizing radiation and the macroscopic biological effects [36, 37]. The establishment of a computational model for predicting DNA damage yield lays a foundation for construction of RBE model and can aid in establishing a more accurate ion-beam RBE model to enhance clinical practice. Compared with the original LNDM, the mLNDM was constructed based on the cumulative probability of DNA DSBs,

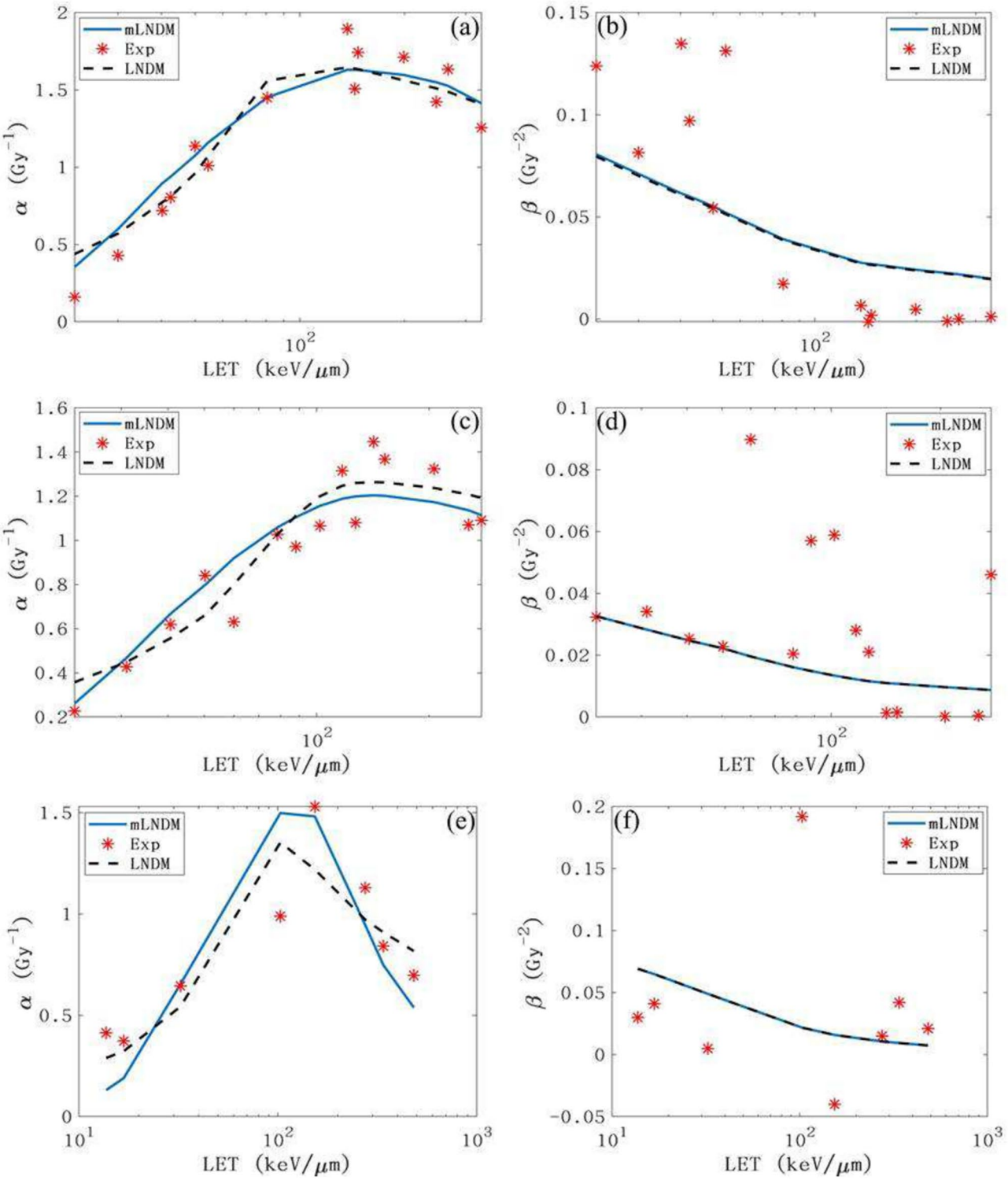

Fig. 3 (Color online) Comparison of the LQ coefficient parameters of the mLNDM calculations, LNDM calculations, and experimental data for HSG (**a** and **b**), V79 cells (**c** and **d**) and CHO-K1 (**e** and **f**) over a wide range of LET values. The symbols show the experimental data extracted from the studies by Furusawa et al. and Weyrather et al., the lines show the mLNDM calculations, and the dashed lines show the LNDM calculations

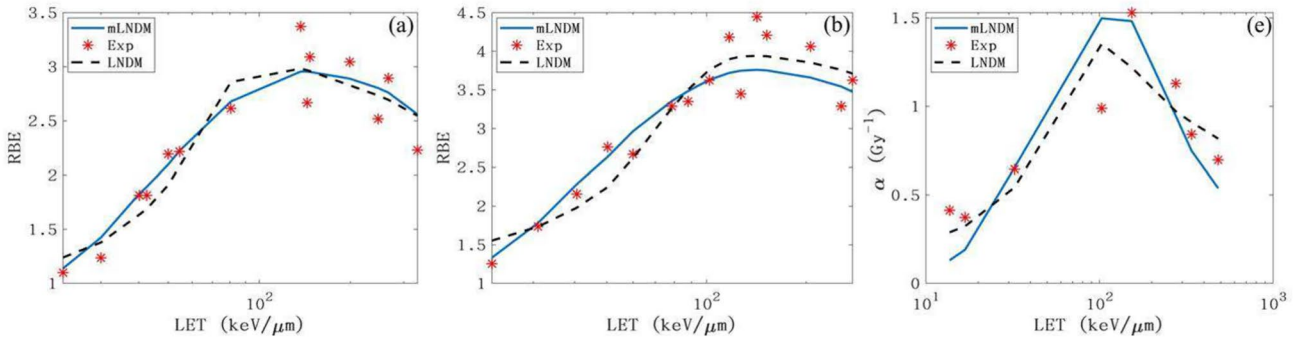

Fig. 4 (Color online) Experimental data and RBE calculated using the mLNDM and LNDM for HSG (**a**), V79 (**b**), and CHO-K1 (**c**) cells, where the experimental data were extracted from the publication of Furusawa et al. and Weyrather et al

Table 2 Determination coefficients R^2 of the experimentally derived data and calculated α, β and RBE values from mLNDM and LNDM for HSG, V79, and CHO-K1 cells

	α-mLNDM	β-mLNDM	RBE-mLNDM	α-LNDM	β-LNDM	RBE-LNDM
HSG	0.91	0.52	0.91	0.91	0.51	0.88
V79	0.85	−0.20	0.89	0.87	−0.20	0.89
CHO-K1	0.57	−0.18	0.81	0.71	−0.18	0.90

thereby improving our understanding of the mechanisms of radiation-induced biological effects. Early random ionization, ionization-induced DNA DSBs, and cell death are included in the modified model. In addition, ionization caused by radiation with different qualities has various biological effects [38]. The introduction of F_{DSB} is significant for the application of the LNDM to other ion species.

In the mLNDM, the α term in the LQ model corresponded to a direct lethal event in the LNDM, and the β term corresponded to an indirect lethal event. Compared with the cumbersome derivation of the LNDM, the mLNDM employs a more direct method to connect both events. In addition, unlike the LNDM, the calculation of indirect lethal events in the mLNDM is based on the method of the β term in the LQ model (the number of DSBs generated by the damage accumulation is proportional to the square of the physical absorbed dose); that is, the number of indirect lethal events is proportional to the square of the number of sublethal events. Compared with the specific derivation results of the LNDM (except for F_2 being replaced by F_{DSB}), the formulation of the α term in the mLNDM model is the first term of the α formulation in the LNDM, and the β terms are identical. The α formulation in the LNDM has three parts. Except for the first term, which is the same as in the α formulation of the mLNDM, the other two terms both contain the parameter $P_{s\to l}$, and the value of $P_{s\to l}$ is extremely small. (The order of magnitude is 10^{-11}.) Therefore, the calculated results for these two terms are negligible compared with the first term. Therefore, the mLNDM simplifies the method of calculating the carbon-ion beam RBE value.

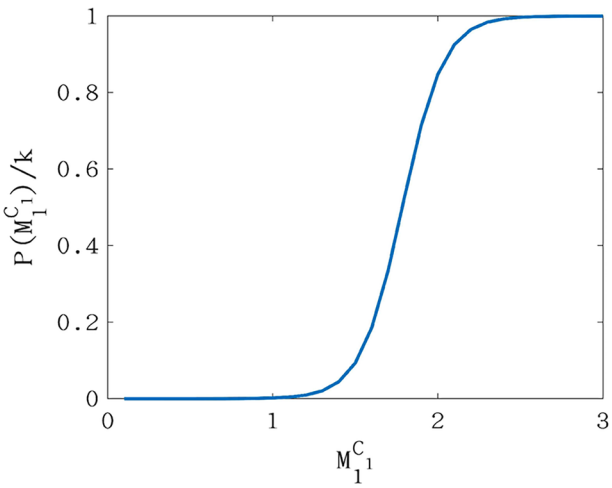

Fig. 5 (Color online) Plot of the logistic function in the mLNDM

In addition, during the optimization of the mLNDM parameters, we observed that parameters r and m_0 have no relation with cell type. Thus, the shape of the logistic function $P\left(M_1^{C_1}\right)/k$ is independent of cell radiosensitivity, as shown in Fig. 5. Some researchers observed that the optimal nanodosimetric quantity for describing the probability of DNA strand breaks is different for various ion species [38].

The guesswork parameters r and m_0 are related to ion species. The parameter k can be used to characterize the radiosensitivity of different cell types. Previous studies have shown that parameter k reflects the proportion of the critical target volume in the cell nucleus, and the lower the percentage, the stronger the radiation resistance [39]. This explanation is consistent with the optimization results in this study. When calculating RBE values for cells with different radiosensitivities, a reduction in modeling parameters is more conducive for revealing the relationship between nanodosimetric quantities and biological effects of radiation. Note that this study only verified the above results with the experimental data of HSG, V79, and CHO-K1 cells under aerobic conditions, thus providing a new approach for the optimization of free parameters for the LNDM. Using experimental data from the other cell lines, the conclusions of this study can be further verified.

The mLNDM accurately reproduced the radiobiological experimental data for HSG, V79, and CHO-K1 cells under aerobic conditions. Currently, only the RBE value of carbon-ion beam has been evaluated using the LNDM and its modification. To expand the scope of application of the model, we must further investigate the applicability of the LNDM to other ion species. For example, the influence of ion species on the model parameters r and m_0, and the influence of the distance between sublethal events under different ion irradiation conditions on probability $P_{s\to l}$ should be considered. In addition, to obtain more realistic nanodosimetric data, several problems in track-structure MC simulations must be further studied. In this study, a simplified chromatin fiber model of DNA, as established by Bueno et al., was introduced into the track-structure MC simulation. In the future, more precise and accurate DNA models should be developed to acquire more accurate MC simulation data. Furthermore, in this study, the track-structure MC simulations considered only the physical process. For reasons of the authenticity of ICSDs, the subsequent radiobiological processes such as chemical and biological stages. Eventually, for the applicability of the model, radiobiological experiments should be conducted under various radiation scenarios.

5 Conclusion

Nuclear DNA damage is the most important type of primary damage caused by radiation. In this study, the LNDM was modified based on DNA distribution of strand break clusters, thereby forming a modified LNDM (mLNDM). The parameters of the mLNDM were optimized using radiobiological experimental data available for HSG, V79, and CHO-K1 cells at different radiosensitivities. The optimization results showed that the modeling parameters r and m_0 are independent of cell type; that is, only the other two parameters, k and $P_{s\to l}$, can be used to depict the radiosensitivity of the different cell lines. In addition, compared with the LNDM, the mLNDM eliminates the tedious derivation process, simplifies the calculation method for RBE, and relates nanodosimetric quantities to biological effects in a direct and easy-to-understand manner. The mLNDM reproduces radiobiological experimental data well and more directly reveals the mechanisms of radiation biological effects. This is significant for understanding and calculating the RBE values of ion beams, thereby providing simple and accurate computation method of RBE value for ion-beam treatment planning.

Author Contributions All authors contributed to the study conception and design. Material preparation, data collection, and analysis were performed by Jing-Fen Yang. The first draft of the manuscript was written by Jing-Fen Yang, and all authors commented on previous versions of the manuscript. All authors read and approved the final manuscript.

Data availability The data that support the findings of this study are openly available in Science Data Bank at https://cstr.cn/31253.11.sciencedb.j00186.00484 and https://doi.org/10.57760/sciencedb.j00186.00484.

Declarations

Conflict of interest The authors declare that they have no conflict of interest.

References

1. G.Q. Xiao, Q. Li, J. Xia et al., The development and commercialization of carbon ion cancer therapy facility. Sci. Technol. Dev. **16**, 9–17 (2020). (**in Chinese**)
2. Q. Li, Biomedical research with heavy ions at the IMP accelerators. Adv. Space Res. **40**, 455–460 (2007). https://doi.org/10.1016/j.asr.2007.03.096
3. Z.Y. Dai, Q. Li, X.G. Liu et al., Active spot-scanning test with heavy ions at HIRFL-CSR. Chin. Phys. C **36**, 784–791 (2012). https://doi.org/10.1088/1674-1137/36/8/018
4. Q. Li, Z.Y. Dai, Z. Yan et al., Heavy-ion conformal irradiation in the shallow-seated tumor therapy terminal at HIRFL. Med. Biol. Eng. Comput. **45**, 1037–1043 (2007). https://doi.org/10.1007/s11517-007-0245-3
5. Q. Li, L. Sihver, Therapeutic techniques applied in the heavy-ion therapy at IMP. Nucl. Instrum. Meth. B. **269**, 664–670 (2011). https://doi.org/10.1016/j.nimb.2011.01.125
6. Q. Li, X.G. Liu, Z.Y. Dai et al., Progress in heavy ion cancer therapy at IMP, in *Proceedings of the 8th China-Japan Joint Nucl. Phys. Syposium (CJJNPS), China Inst Atom Energy (CIAE)*, Beijing, China, Oct 15–19, 2012. https://doi.org/10.1063/1.4806796
7. G.Q. Xiao, H. Zhang, Q. Li et al., Progresses of heavy-ion cancer therapy in IMP. Nucl. Phys. Rev. **24**, 85–88 (2007). (**in Chinese**)
8. G.Q. Xiao, Z.Z. Li, Heavy ion research facility. Bull. Chin. Acad. Sci. **24**, 97–105 (2009). https://doi.org/10.16418/j.issn.1000-3045.2009.01.003. (**in Chinese**)
9. T. Kanai, N. Matsufuji, T. Miyamoto et al., Examination of GyE system for HIMAC carbon therapy. Int. J. Radiat. Oncol. Biol. Phys. **64**, 650–656 (2006). https://doi.org/10.1016/j.ijrobp.2005.09.043
10. C.P. Karger, C. Glowa, P. Peschke et al., The RBE in ion beam radiotherapy. In Vivo studies and clinical application. Z. Med.

Phys. **31**, 105–121 (2021). https://doi.org/10.1016/j.zemedi.2020.12.001
11. X.G. Liu, Q. Li, Z.Y. Dai et al., Method of dose calculation for heavy-ion cancer therapy at IMP. Nucl. Phys. Review. **26**, 69–75 (2009). (**in Chinese**)
12. M. Zaider, H.H. Rossi, The synergistic effects of different radiations. Radiat. Res. **83**, 732–739 (1980). https://doi.org/10.2307/3575352
13. R.B. Hawkins, A microdosimetric-kinetic model of cell death from exposure to ionizing radiation of any LET, with experimental and clinical applications. Int. J. Radiat. Biol. **69**, 739–755 (1996). https://doi.org/10.1080/095530096145481
14. M. Scholz, A.M. Kellerer, W. KraftWeyrather et al., Computation of cell survival in heavy ion beams for therapy—the model and its approximation. Radiat. Environ. Biophys. **36**, 59–66 (1997). https://doi.org/10.1007/s004110050055
15. T.Y. Dai, Q. Li, X.G. Liu et al., Nanodosimetric quantities and RBE of a clinically relevant carbon-ion beam. Med. Phys. **47**, 772–780 (2020). https://doi.org/10.1002/mp.13914
16. V. Conte, A. Selva, P. Colautti et al., Track structure characterization and its link to radiobiology. Radiat. Meas. **106**, 506–511 (2017). https://doi.org/10.1016/j.radmeas.2017.06.010
17. B. Grosswendt, Nanodosimetry, from radiation physics to radiation biology. Radiat. Prot. Dosim. **115**, 1–9 (2005). https://doi.org/10.1093/rpd/nci152
18. T. Li, W. Li, T. Lu et al., Current status of of nanodosimetry. Chin. J. Radiol. Med. Protect. **41**, 784–789 (2021). https://doi.org/10.3760/cma.j.issn.0254-5098.2021.10.011. (**in Chinese**)
19. Y. Fu, P. Li, From microdosimetry to nanodosimetry-the link between radiobiology and radiation physics. J. Biomed. Eng. **31**, 703–707 (2014). https://doi.org/10.7507/1001-5515.20140131. (**in Chinese**)
20. G. Garty, R. Schulte, S. Shchemelinin et al., A nanodosimetric model of radiation-induced clustered DNA damage yields. Phys. Med. Biol. **55**, 761–781 (2010). https://doi.org/10.1088/0031-9155/55/3/015
21. H. Rabus, Nanodosimetry - on the "tracks'' of biological radiation effectiveness. Z. Med. Phys. **30**, 91–94 (2020). https://doi.org/10.1016/j.zemedi.2020.01.002
22. D. Chen, L. Sun, Application of microdosimetry on Aip Conf Proc for ionizing radiation. Chin. Phys. B **27**, 028701 (2018). https://doi.org/10.1088/1674-1056/27/2/028701
23. R.W. Schulte, A.J. Wroe, V.A. Bashkirovz et al., Nanodosimetry-based quality factors for Radiat. Prot. space. Z. Med. Phys. **18**, 286–296 (2008). https://doi.org/10.1016/j.zemedi.2008.06.011
24. S. Kapoor, C. Gopinathan, Calculations on high LET radiation tracks. J. Radioan. Nucl. Ch. Ar. **150**, 3–13 (1991). https://doi.org/10.1007/bf02041486
25. M. Casiraghi, R.W. Schulte, Nanodosimetry-based plan optimization for particle therapy. Comput. Math. Method. M. **2015**, 908971 (2015). https://doi.org/10.1155/2015/908971
26. Y. Feng, S. He, T. Liu, Linear quadratic model and its clinical significance. Chin. J. Radiat. Oncol. 65–69 (1988). (in Chinese)
27. W. Yang, N. Feng, Y. Shen, Biological concept and application of LQ formula. Chin. J. Radiat. Oncol. 59–63 (1995) (**in Chinese**)
28. Y. Furusawa, K. Fukutsu, M. Aoki et al., Inactivation of aerobic and hypoxic cells from three different cell lines by accelerated ^{3}He-, ^{12}C- and ^{20}Ni-ion beams. Radiat. Res. **154**, 485–496 (2000). http://www.jstor.org/stable/3580658
29. W.K. Weyrather, S. Ritter, M. Scholz et al., RBE for carbon track-segment irradiation in cell lines of differing repair capacity. Int. J. Radiat. Biol. **75**, 1357–1364 (1999). https://doi.org/10.1080/095530099139232
30. J. Perl, J. Shin, J. Schumann et al., TOPAS: an innovative proton Monte Carlo platform for research and clinical applications. AIP Conf. Proc. **39**, 6818–6837 (2012). https://doi.org/10.1118/1.4758060
31. L. Yang, Investigation of the impact of magnetic field on multi-particle radiation dose in MRIgRT using Monte Carlo software TOPAS. University of Science and Technology of China (2018). (**in Chinese**)
32. J. Schuemann, A.L. McNamara, J. Ramos-Mendez et al., Topas-nbio: an extension to the TOPAS simulation toolkit for cellular and sub-cellular radiobiology. Radiat. Res. **191**, 125–138 (2019). https://doi.org/10.1667/rr15226.1
33. M. Bueno, R. Schulte, S. Meylan et al., Influence of the geometrical detail in the description of DNA and the scoring method of ionization clustering on nanodosimetric parameters of track structure: a Monte Carlo study using Geant4-DNA. Phys. Med. Biol. **60**, 8583–8599 (2015). https://doi.org/10.1088/0031-9155/60/21/8583
34. D.T. Goodhead, Initial events in the cellular effects of ionizing-radiations - clustered damage in DNA. Int. J. Radiat. Biol. **65**, 7–17 (1994). https://doi.org/10.1080/09553009414550021
35. D.T. Goodhead, Energy deposition stochastics and track structure: what about the target? Radiat. Prot. Dosim. **122**, 3–15 (2006). https://doi.org/10.1093/rpd/ncl498
36. X. Jiang, Research on nanodosimetry Ann Ny Acad Sci and repair module based on the DNA atomic model. Tsinghua University (2016). (**in Chinese**)
37. D. Kong, Research of impact factors of nanodosimetric DNA model. Soochow University (2014). (**in Chinese**)
38. M.U. Bug, G. Hilgers, W.Y. Baek et al., Nanodosimetric characterization of ion beams. Eur. Phys. J. D **68**, 217 (2014). https://doi.org/10.1140/epjd/e2014-50015-9
39. T.Y. Dai, Research on the relative biological effectiveness of ion beams based on microdosimetry and nanodosimetry. University of Chinese Academy of Sciences (Institute of Modern Physics, Chinese Academy of Sciences) (2020). (**in Chinese**)